



Characterization of focal liver lesions using the stretched exponential model: comparison with monoexponential and biexponential diffusion-weighted magnetic resonance imaging

Hyung Cheol Kim¹ · Nieun Seo¹ · Yong Eun Chung¹ · Mi-Suk Park¹ · Jin-Young Choi¹ · Myeong-Jin Kim¹

Received: 30 September 2018 / Revised: 23 December 2018 / Accepted: 25 January 2019 / Published online: 22 February 2019
© European Society of Radiology 2019

Abstract

Objective To compare the stretched exponential model of diffusion-weighted imaging (DWI) with monoexponential and biexponential models in terms of the ability to characterize focal liver lesions (FLLs).

Methods This retrospective study included 180 patients with FLLs who underwent magnetic resonance imaging including DWI with nine b values at 3.0 T. The distributed diffusion coefficient (DDC) and intravoxel diffusion heterogeneity index (α) from a stretched exponential model; true diffusion coefficient (D_t), pseudo-diffusion coefficient (D_p), and perfusion fraction (f) from a biexponential model; and apparent diffusion coefficient (ADC) were calculated for each lesion. Diagnostic performances of the parameters were assessed through receiver operating characteristic (ROC) analysis. For 20 patients with treated hepatic metastases, the correlation between the DWI parameters and the percentage of tumor necrosis on pathology was evaluated using the Spearman correlation coefficient.

Results DDC had the highest area under the ROC curve (AUC, 0.905) for differentiating malignant from benign lesions, followed by D_t (0.903) and ADC (0.866), without significant differences among them (DDC vs. D_t , $p = 0.946$; DDC vs. ADC, $p = 0.157$). For distinguishing hypovascular from hypervascular lesions, and hepatocellular carcinoma from metastasis, f had a significantly higher AUC than the other DWI parameters ($p < 0.05$). The α had the strongest correlation with the degree of tumor necrosis ($\rho = 0.655$, $p = 0.002$).

Conclusion The DDC from stretched exponential model of DWI demonstrated excellent diagnostic performance for differentiating malignant from benign FLLs. The α is promising for evaluating the degree of necrosis in treated metastases.

Key Points

- The stretched exponential DWI model is valuable for characterizing focal liver lesions.
- The DDC from stretched exponential model shows excellent performance for differentiating malignant from benign focal liver lesions.
- The α from stretched exponential model is promising for evaluating the degree of necrosis in hepatic metastases after chemotherapy.

Keywords Liver · Hepatocellular carcinoma · Metastasis · Diffusion magnetic resonance imaging · Comparative study

Abbreviations

ADC Apparent diffusion coefficient
AUC Area under the ROC curve

CI Confidence interval
DDC Distributed diffusion coefficient
DWI Diffusion-weighted imaging
EHE Epithelioid hemangioendothelioma
FLL Focal liver lesion
FNH Focal nodular hyperplasia
HCC Hepatocellular carcinoma
ICC Intrahepatic cholangiocarcinoma
IVIM Intravoxel incoherent motion
MRI Magnetic resonance imaging
ROC Receiver operating characteristic

✉ Nieun Seo
sldmsdl@yuhs.ac

¹ Department of Radiology, Severance Hospital, Yonsei University College of Medicine, 50 Yonsei-ro, Seodaemun-gu, Seoul 03722, South Korea

ROI Region of interest
T2WI T2-weighted imaging

Introduction

Diffusion-weighted imaging (DWI) is a widely used magnetic resonance imaging (MRI) sequence that is helpful for the detection and characterization of focal liver lesions (FLLs) [1, 2]. DWI reflects tissue diffusibility in FLLs, and this characteristic can be quantified by the apparent diffusion coefficient (ADC) obtained using the monoexponential model of DWI data. Although previous studies have shown the usefulness of ADC in the characterization of FLLs, considerable overlaps have been observed in the ADC values of benign and malignant liver lesions [1–5]. Because both true molecular diffusion and blood perfusion affect ADC values, the ADC may not represent true tissue characteristics [6]. Intravoxel incoherent motion (IVIM), a biexponential model of DWI with multiple b values, enables the separate analysis of pure molecular diffusion and blood perfusion [7]. In prior studies, the true diffusion coefficient (D_t) obtained from the IVIM model demonstrated better diagnostic performance than the ADC in the differentiation of benign and malignant hepatic lesions [6, 8]. In addition, the perfusion fraction (f) and pseudo-diffusion coefficient (D_p) were useful for evaluating the hypervascularity of FLLs [6, 8].

However, the biexponential model has been criticized for oversimplification of diffusion parameters to only two compartments, i.e., true diffusion and perfusion compartments [9, 10]. Stretched exponential model can overcome the limitations of the hypothesis of two diffusion compartments in a biexponential model, by not assuming the specific number of different compartments. Instead, the stretched exponential model considers the composite of continuous distribution of ADCs in each part. Therefore, stretched exponential model is thought to reflect physiologic characteristics of biologic tissue, considering the heterogeneity of intravoxel diffusion rates and the distributed diffusion effect within each voxel in multiple pools of water molecules [11]. Several clinical studies have used the stretched exponential model [12–17]. For characterizing liver disease, several investigators have reported the usefulness of the stretched exponential model in evaluating hepatic fibrosis [12, 18]. To our knowledge, only one recent study has compared different DWI models for differentiating benign from malignant hepatic lesions [19]. Differentiation of malignant from benign FLLs is also available on contrast-enhanced computed tomography or MRI. However, DWI is particularly useful that it does not require intravenous contrast administration, and different DWI models can reflect different functional characteristics of FLLs. Therefore, it would be meaningful to investigate whether there is an additional value of stretched exponential model of DWI compared with other models in the diagnosis of benign and malignant FLLs. In

addition, for treated metastatic lesions which are composed of viable tumor, fibrosis, and necrosis, increased necrosis after chemotherapy can be interpreted as treatment response. Although there have been several reports that increased ADC and D_t reflected tumor necrosis after chemotherapy [20–22], there has been no study on the role of stretched DWI model for evaluating tumor necrosis in treated metastases.

Therefore, the purpose of our study was to evaluate the ability and potential additional value of the stretched exponential model of DWI for characterization of FLLs compared with those of the monoexponential and biexponential models.

Materials and methods

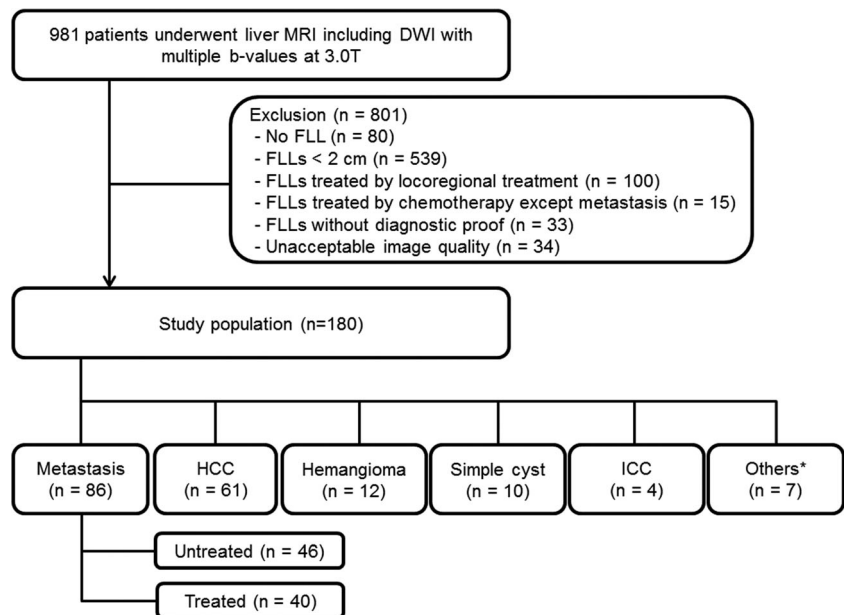
Study population

Our Institutional Review Board approved this retrospective study and waived the requirement for informed patient consent because of its retrospective design. A total of 981 adult patients who underwent liver MRI, including DWI with multiple b values at 3 T, at our hospital between November 2015 and January 2017 were retrospectively recruited. Among these patients, 801 patients were excluded after meeting the following exclusion criteria (Fig. 1): (1) patients without any FLLs ($n = 80$), (2) patients with FLLs less than 2 cm in diameter ($n = 539$); (3) patients who underwent locoregional treatment for hepatic tumors prior to MRI ($n = 100$); (4) patients undergoing chemotherapy for hepatic tumors except metastases ($n = 15$); (5) patients without diagnostic proof of FLLs ($n = 33$), and (6) patients with unacceptable DWI image quality for evaluating FLLs ($n = 34$). Finally, 180 patients were included in this study (male:female, 122:58; mean age, 57.4 ± 11.5 years). For patients with more than one hepatic lesion, only the largest was included for analysis to avoid a clustering effect within the patient. The final diagnoses of the FLLs were hepatocellular carcinoma (HCC) in 61 patients, metastasis in 86, hemangiomas in 12, simple hepatic cysts in 10, intrahepatic cholangiocarcinoma (ICC) in 4, focal nodular hyperplasia (FNH) in 3, combined hepatocellular-cholangiocarcinoma (cHCC-CC) in 1, epithelioid hemangioendothelioma (EHE) in 1, angiomyolipoma in 1, and abscess in 1. Among the 86 patients with hepatic metastasis, 40 patients were treated with systemic chemotherapy. Treated metastases were only included in the analysis of the correlation between DWI parameters and tumor necrosis. The diameter of the FLLs ranged from 2.0 to 20.0 cm, with a mean diameter of 4.66 cm (Table 1).

Confirmation of hepatic lesions

Among the 180 FLLs, 89 lesions were pathologically confirmed by biopsy ($n = 23$) or surgery ($n = 66$), and the

Fig. 1 Flowchart of the study population. *Others included three focal nodular hyperplasias, one combined hepatocellular and cholangiocarcinoma, one epithelioid hemangioendothelioma, one angiomyolipoma, and one abscess. MRI, magnetic resonance imaging; DWI, diffusion-weighted imaging; FLL, focal liver lesion; HCC, hepatocellular carcinoma; ICC, intrahepatic cholangiocarcinoma



remaining 91 were diagnosed based on typical clinical and MRI findings with at least 6 months of follow-up (Table 1). The diagnostic MRI criteria of FLLs without pathologic confirmation were as follows: (1) HCCs were diagnosed when lesions exhibited arterial hyperenhancement and venous or delayed phase washout in high-risk patients, according to the criteria proposed by the American Association for the Study of Liver Disease [23]; (2) metastases were diagnosed when the lesions exhibited peripheral rim enhancement and a diameter increase of at least 20% during serial imaging follow-up in patients with a known primary malignancy [8, 24]; (3) hemangiomas were defined when lesions exhibited high signal intensity on T2-weighted imaging (T2WI) and a typical dynamic enhancement pattern without interval change during at least 6 months of follow-up; (4) hepatic cysts were diagnosed when lesions exhibited bright signal intensity on T2WI without contrast enhancement; (5) FNH were diagnosed based on typical MRI findings of a hyperintense central scar on T2WI, rapid and strong arterial hypervascularity, and retention of contrast medium in the hepatobiliary phase using gadoxetate-enhanced MRI [25]; and (6) abscess was diagnosed based on peripheral enhancing multiseptated cystic lesions in a clinical setting with fever and chills [26].

MRI acquisition

MRI was performed on a 3-T machine (Achieva TX, or Ingenia; Philips Healthcare) using anterior and posterior coils. The routine MRI protocol consisted of dual-echo spoiled gradient-echo T1-weighted in-phase and opposed-phase images, multi-shot and single-shot turbo spin-echo T2WI, free breathing single-shot echo-planar DWI, and dynamic fat-suppressed spoiled gradient-echo T1WI before and after the

injection of contrast medium. The DWI was acquired with the following parameters: echo time, 50.2 ms; repetition time, 5000 ms; echo train length, 27; receiver bandwidth, 2877 per pixel; field of view, 400 mm; matrix size, 90×92 ; number of excitations, 3; section thickness, 5 mm; spectral adiabatic inversion-recovery fat suppression; acquisition time, approximately 4 min 15 s. Three orthogonal spatial directions were encoded with nine diffusion-weighted gradients: b values of 0, 10, 25, 50, 75, 100, 200, 500, and 800 s/mm^2 .

Post-processing and image analysis

DWI data were analyzed using IVIM post-processing software (EXPRESS; Philips Healthcare) to acquire DWI parameters and parametric maps. The DWI parameters were calculated according to the following mathematical models: where $S(b)$ is the signal intensity under the given b value and $S(0)$ represents the signal intensity for $b = 0$ s/mm^2 . All nine b values were used as input data.

In the monoexponential model, the ADC was calculated using the monoexponential linear fitting (least-square) technique on a pixel-by-pixel basis with the following equation:

$$S(b)/S(0) = \exp(-b \cdot \text{ADC})$$

In the biexponential model, DWI signal decay was expected to follow the IVIM model. The true diffusion coefficient (D_t) was obtained using b values > 200 s/mm^2 with the simple linear fit equation. The pseudo-diffusion coefficient (D_p) and perfusion fraction (f) were then calculated with a nonlinear regression algorithm [7].

$$S(b)/S(0) = [(1-f) \cdot \exp(-b \cdot D_t)] + [f \cdot \exp(-b \cdot D_p)]$$

Table 1 Number and reference standard of focal liver lesions

Focal liver lesions	Number	Mean size (cm)	Reference standard		
			Biopsy	Surgery	Imaging
HCC	61	5.05 ± 3.18	6	24	31
Metastasis (untreated)	46	4.41 ± 3.17	8	21	17
Metastasis (treated)*	40	4.36 ± 3.25	5	16	19
Hemangioma	12	4.12 ± 3.23	0	1	11
Cyst	10	4.79 ± 3.26	0	1	9
Intrahepatic cholangiocarcinoma	4	6.35 ± 3.24	3	1	0
Focal nodular hyperplasia	3	4.27 ± 3.16	0	0	3
Abscess	1	4.10	0	0	1
Angiomyolipoma	1	6.20	0	1	0
EHE	1	2.50	0	1	0
cHCC-CC	1	5.20	1	0	0
Total	180	4.66 ± 3.20	23	66	91

Sizes are presented as the mean diameter ± standard deviation

HCC, hepatocellular carcinoma; EHE, epithelioid hemangioendothelioma; cHCC-CC, combined hepatocellular carcinoma and cholangiocarcinoma

*Treated metastases were only included for analysis of correlation between tumor necrosis and diffusion-weighted parameters

In the stretched exponential model, the distributed diffusion coefficient (DDC) and the water molecular diffusion heterogeneity index (α) were acquired using the following equation [11]:

$$S(b)/S(0) = \exp[-(b \cdot \text{DDC})^\alpha]$$

where DDC indicates the mean intravoxel diffusion rate and α represents intravoxel water molecular diffusion heterogeneity, ranging from 0 to 1. For the biexponential and stretched exponential models, the Levenberg–Marquardt fit was used [13].

For quantitative analysis, one junior radiology resident (H.C.K.) performed region of interest (ROI) measurement under the supervision of a board-certified abdominal radiologist (N.S., with 5 years of experience in liver MRI), and both radiologists were unaware of the clinicopathologic findings. ROIs were drawn on DWI images ($b = 0 \text{ s/mm}^2$) using post-processing software to include the largest area and the most representative portion of the FLL on three consecutive DWI images. The mean area of the ROIs was $1973 \pm 3537 \text{ mm}^2$. The average of the three ROI values was used for statistical analysis.

For qualitative analysis, the vascularity of FLLs was reviewed by consensus of two radiologists (Y.E.C. and N.S., with 10 and 5 years of clinical experience in liver MRI, respectively). After the exclusion of hepatic cysts and treated metastases, 130 FLLs were divided into groups of hypovascular ($n = 61$) and hypervascular lesions ($n = 69$). The vascularity of the FLLs was determined based on the relative enhancement of the dominant part (> 50%) within the lesions compared with that of the background liver in the

late arterial phase. The hypovascular FLLs consisted of metastases ($n = 40$), HCCs ($n = 8$), hemangiomas ($n = 6$), ICCs ($n = 4$), abscess ($n = 1$), EHE ($n = 1$), and cHCC-CC ($n = 1$). The hypervascular FLLs included HCCs ($n = 53$), metastases ($n = 6$), hemangiomas ($n = 6$), FNH ($n = 3$), and angiomyolipoma ($n = 1$).

Statistical analysis

All DWI parameters were compared according to the lesion diagnoses using the independent sample *t* test or analysis of variance with the Bonferroni multiple comparisons as a post hoc test. Because the numbers of ICC ($n = 4$), FNH ($n = 3$), abscess ($n = 1$), angiomyolipoma ($n = 1$), EHE ($n = 1$), and cHCC-CC ($n = 1$) were too small for a separate statistical analysis, these FLLs were excluded from the aforementioned analysis. Instead, these FLLs were included in the following analyses. The independent sample *t* test was used to compare DWI parameters in solid FLLs between benign and malignant lesions and between hypovascular and hypervascular lesions. For the evaluation of benign solid FLLs, cysts were excluded, and hemangiomas were included in the analysis. The diagnostic performances of the DWI parameters in differentiating solid FLLs were evaluated using receiver operating characteristic (ROC) analysis and the area under the ROC curve (AUC). The AUCs among the DWI parameters were compared using the DeLong test. The sensitivity and specificity of the DWI parameters were calculated at the cutoff values that can achieve the largest Youden index. For the surgically confirmed hepatic metastases treated with chemotherapy, the correlation of the

DWI parameters and the degree of tumor necrosis based on pathologic reports was evaluated using the Spearman correlation coefficient. Statistical analyses were performed using the SPSS v23.0 software (IBM Corp.) and MedCalc Statistical Software version 18.2.1 (MedCalc Software Bvba). *P* values < 0.05 were considered statistically significant.

Results

DWI parameter values according to diagnosis

The DWI parametric values of the various FLLs are summarized in Table 2 and Fig. 2. The ADC ($p < 0.001$), D_t ($p < 0.001$), f ($p = 0.005$), and DDC ($p < 0.001$) differed significantly among HCCs, metastases, and hemangiomas. In post hoc comparisons, the ADC, D_t , and DDC of hemangiomas were significantly higher than those of HCCs or metastases ($p < 0.001$). In the comparison between HCCs and metastases, f was significantly higher in HCCs (22.80%) than in metastases (17.06%; $p = 0.004$), but other parameters were not significantly different ($p > 0.05$). In the comparison between hemangiomas and cysts, ADC ($p < 0.001$), D_t ($p = 0.001$), f ($p = 0.003$), DDC ($p = 0.017$), and α ($p = 0.001$) were significantly different. The α was significantly higher in cysts (0.95) than in hemangiomas (0.70). Representative figures of HCC and hemangiomas are shown in Figs. 3 and 4.

Comparison of DWI parameters for discrimination of solid focal lesions according to malignancy and vascularity

The malignant FLLs had significantly lower values of ADC ($p < 0.001$), D_t ($p < 0.001$), and DDC ($p < 0.001$) than the benign FLLs. Conversely, α , f , and D_p were not significantly different between the malignant and benign lesions.

Significant differences were observed in f and α between the two groups, distinguishing hypovascular from hypervascular solid lesions. The f was significantly higher in hypervascular lesions than in hypovascular lesions (24.38% vs. 16.29%, $p < 0.001$), as was α (0.68 vs. 0.60, $p = 0.002$) (Table 3).

Diagnostic performance of DWI parameters in the differentiation of solid focal lesions

Table 4 summarizes the results of ROC analysis for the differentiation of solid FLLs. For the differentiation of malignant lesions from benign lesions, DDC had the largest AUC (0.905; 95% confidence interval [CI], 0.841–0.949) followed by D_t (0.903; 95% CI, 0.838–0.948) and ADC (0.866, 95% CI, 0.795–0.920). The sensitivity and the specificity of DDC for differentiating malignant and benign lesions were 85.8% and 82.4%, respectively, at an optimal cutoff value of $1.785 \times 10^{-3} \text{ mm}^2/\text{s}$. The AUC of DDC was not significantly different from those of D_t ($p = 0.946$) and ADC ($p = 0.157$). Regarding lesion vascularity, f had the largest AUC (0.762; 95% CI, 0.679–0.832), followed by α (0.664; 95% CI, 0.576–0.744) and D_p (0.608; 95% CI, 0.518–0.692). The f had significantly higher AUCs than all other DWI parameters ($p \leq 0.031$). For the differentiation of HCCs from metastases, f also had the largest AUC (0.714; 95% CI, 0.618–0.797), differing significantly from all other DWI parameters ($p \leq 0.019$).

Correlation between DWI parameters and tumor necrosis in treated metastasis

Among the patients with metastases treated with chemotherapy ($n = 40$), 20 patients underwent surgical resection within 1 month after MRI. Correlation of the DWI parameters and the percentage of tumor necrosis reported on the pathologic reports ($n = 20$) was analyzed using the Spearman correlation coefficient (ρ). The α had the strongest correlation with the degree of tumor necrosis

Table 2 Diffusion-weighted imaging parametric values of focal liver lesions

Parameter	HCC ($n = 61$)	Metastasis ($n = 46$)	Hemangioma ($n = 12$)	<i>p</i> value*	Cyst ($n = 10$)	<i>p</i> value†
ADC ($10^{-3} \text{ mm}^2/\text{s}$)	1.33 ± 0.23	1.38 ± 0.4	1.94 ± 0.34	< 0.001	3.12 ± 0.75	< 0.001
D_t ($10^{-3} \text{ mm}^2/\text{s}$)	1.04 ± 0.31	1.17 ± 0.58	1.75 ± 0.31	< 0.001	2.93 ± 0.82	0.001
f (%)	22.80 ± 8.70	17.06 ± 8.26	20.34 ± 11.64	0.005	5.97 ± 6.84	0.003
D_p ($10^{-3} \text{ mm}^2/\text{s}$)	83.69 ± 62.89	84.64 ± 64.21	85.53 ± 56.12	0.994	61.13 ± 62.45	0.346
DDC ($10^{-3} \text{ mm}^2/\text{s}$)	1.32 ± 0.41	1.35 ± 0.53	2.43 ± 0.84	< 0.001	3.24 ± 0.56	0.017
α	0.62 ± 0.14	0.65 ± 0.14	0.70 ± 0.21	0.236	0.95 ± 0.71	0.001

Data are means ± standard deviation

DWI, diffusion-weighted imaging; ADC, apparent diffusion coefficient; D_t , true diffusion coefficient; D_p , pseudo-diffusion coefficient; f , perfusion fraction; DDC, distributed diffusion coefficient; α , intravoxel diffusion heterogeneity index; HCC, hepatocellular carcinoma

*DWI parameters of HCC, metastasis, and hemangiomas were compared using an analysis of variance

† DWI parameters of hemangiomas and cysts were compared using an independent sample *t* test

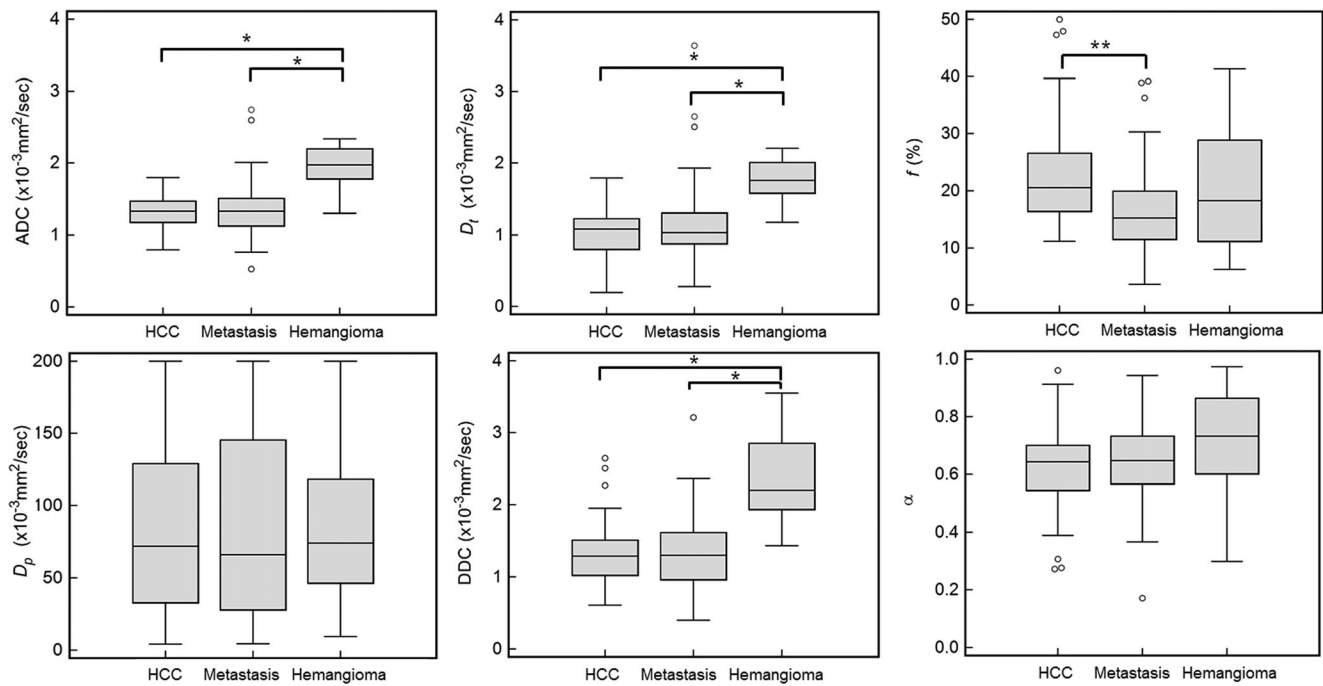


Fig. 2 Box plots of diffusion-weighted imaging parameters of hepatocellular carcinoma (HCC), metastasis, and hemangiomas. $*p < 0.001$ and $**p = 0.004$. D_p and α did not differ significantly among HCC, metastasis, and hemangioma

($\rho = 0.655$, $p = 0.002$), followed by D_t ($\rho = 0.576$, $p = 0.008$) (Figs. 5 and 6). The other DWI parameters were not significantly correlated with the degree of tumor necrosis.

Discussion

The results of this study showed that the DDC from the stretched exponential model demonstrated the optimal

diagnostic performance in differentiating malignant from benign FLLs, followed by D_t and ADC, although the differences among them were not significant. A recent study also showed that DDC had the highest value (AUC, 0.819) in distinguishing between malignant and benign hepatic lesions [19]. This indicates that the average diffusion rate of benign hepatic lesions is higher than that of malignant lesions, and DDC may have the strongest ability to discriminate benign from malignant liver lesions with less overlap. Conversely,

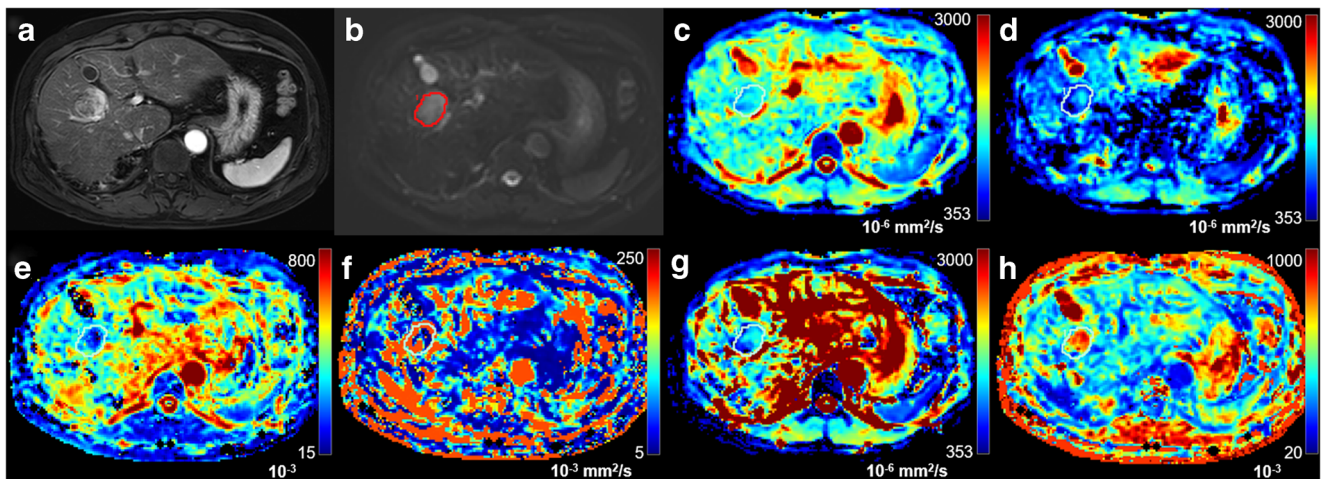


Fig. 3 Imaging of a 65-year-old man with hepatocellular carcinoma (HCC). **a** Axial T1-weighted image acquired during the arterial phase showing a hyperenhancing mass in the right anterior section of the liver. **b** The region of interest was manually drawn on the hepatic tumor on the

diffusion-weighted image acquired with a b value of 0 s/mm^2 and copied onto (c–h) color maps. The values of (c) the ADC, (d) D_t , (e) f , (f) D_p , (g) DDC, and (h) α of HCC were $1.23 \times 10^{-3} \text{ mm}^2/\text{s}$, $0.80 \times 10^{-3} \text{ mm}^2/\text{s}$, 26.31%, $165.26 \times 10^{-3} \text{ mm}^2/\text{s}$, $1.20 \times 10^{-3} \text{ mm}^2/\text{s}$, and 0.49, respectively

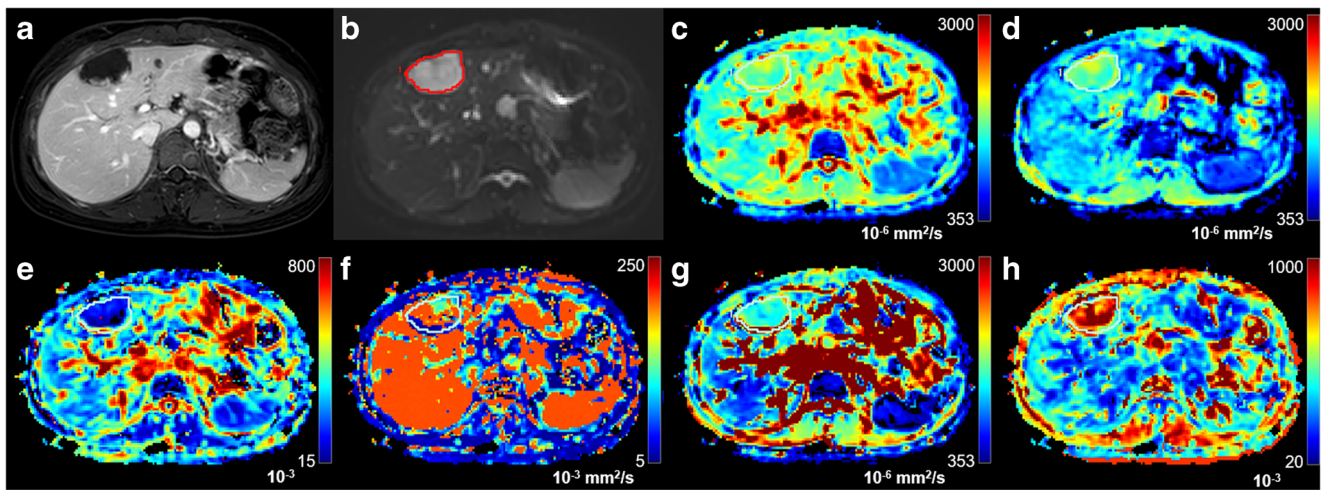


Fig. 4 Imaging of a 38-year-old woman with hemangioma. **a** Axial T1-weighted image acquired during the delayed phase showing peripheral nodular enhancement of a hepatic mass. **b** The region of interest was manually drawn on the hepatic tumor on the diffusion-weighted image

acquired with a b value of 0 s/mm^2 and copied onto (c–h) color maps. The values of (c) the ADC, (d) D_t , (e) f , (f) D_p , (g) DDC, and (h) α of hemangioma were $1.65 \times 10^{-3} \text{ mm}^2/\text{s}$, $1.62 \times 10^{-3} \text{ mm}^2/\text{s}$, 17.15%, $178.28 \times 10^{-3} \text{ mm}^2/\text{s}$, $1.58 \times 10^{-3} \text{ mm}^2/\text{s}$, and 0.79, respectively

the α , another parameter from the stretched exponential model, could not distinguish between benign and malignant liver lesions. The α represents intravoxel water molecular diffusion heterogeneity, ranging from 0 to 1 [11, 13]. A lower α value indicates higher intravoxel diffusion heterogeneity, indicating higher heterogeneity of exponential decay [11]. In a previous study, the α value did not differ significantly between benign and malignant liver lesions, although it could distinguish normal hepatic parenchyma from benign and malignant liver lesions [19]. In a comparison of monoexponential and biexponential DWI models for differentiating malignant from benign lesions, D_t demonstrated better diagnostic performance than conventional ADC [6, 8], which corroborates our study results.

We found that the IVIM-derived perfusion parameter, f , demonstrated the strongest diagnostic performance for differentiating hypervascular liver lesions from hypovascular lesions. The D_p did not differ significantly between

hypervascular and hypovascular liver lesions in this study. Our results are in good agreement with previous studies, which have shown a positive correlation between f and the degree of enhancement in hepatic tumors including HCCs and in renal lesions [6, 8, 27, 28]. The poor reliability of D_p reported in prior studies may explain the poor correlation between D_p and the hypervascularity of the FLLs [6, 8, 12, 29]. In our study, the α value of hypervascular FLLs was significantly lower than that of hypovascular FLLs (0.60 vs. 0.68, $p = 0.002$), although the AUC of α for the differentiation of hypervascular and hypovascular FLLs was significantly lower than that of f . This result may indicate that the hypervascular liver lesions had a higher degree of multiexponential signal decay, possibly because of the prominent vascular structure, angiogenesis, and tissue heterogeneity. One other explanation could be that the HCCs, which comprised the largest portion of hypervascular liver lesions (76.8%, 53/69) in this study, had a lower α value than the other hepatic lesions.

Table 3 Diffusion-weighted imaging parametric values of solid focal liver lesions according to malignancy and vascularity

Parameter	Benign ($n = 17$)	Malignant ($n = 113$)	p value*	Hypovascular ($n = 61$)	Hypervascular ($n = 69$)	p value†
ADC ($10^{-3} \text{ mm}^2/\text{s}$)	1.86 ± 0.33	1.37 ± 0.32	< 0.001	1.41 ± 0.40	1.44 ± 0.33	0.627
D_t ($10^{-3} \text{ mm}^2/\text{s}$)	1.68 ± 0.31	1.10 ± 0.44	< 0.001	1.23 ± 0.56	1.13 ± 0.37	0.221
f (%)	21.45 ± 11.40	20.45 ± 8.90	0.681	16.29 ± 7.27	24.38 ± 9.14	< 0.001
D_p ($10^{-3} \text{ mm}^2/\text{s}$)	83.30 ± 48.30	82.28 ± 63.94	0.939	71.64 ± 60.56	91.94 ± 62.05	0.062
DDC ($10^{-3} \text{ mm}^2/\text{s}$)	2.39 ± 0.82	1.36 ± 0.48	< 0.001	1.44 ± 0.54	1.54 ± 0.71	0.376
α	0.66 ± 0.21	0.64 ± 0.15	0.688	0.68 ± 0.15	0.60 ± 0.15	0.002

Data are means \pm standard deviation. Treated metastasis and cysts were excluded from this analysis

ADC, apparent diffusion coefficient; D_t , true diffusion coefficient; D_p , pseudo-diffusion coefficient; f , perfusion fraction; DDC, distributed diffusion coefficient; α , intravoxel diffusion heterogeneity index

*Differences between benign and malignant solid focal lesions

† Differences between hypovascular and hypervascular solid focal lesions

Table 4 Results of receiver operating characteristic analysis for differentiation of solid liver lesions

	Parameters	Cutoff	Sensitivity	Specificity	AUC	95% CI
Benign* vs. malignant	ADC (10^{-3} mm ² /s)	1.656	88.5	76.5	0.866	0.795, 0.920
	D_t (10^{-3} mm ² /s)	1.400	85.8	82.4	0.903	0.838, 0.948
	f (%)	24.050	74.3	47.1	0.532	0.443, 0.620
	D_p (10^{-3} mm ² /s)	49.845	41.6	82.4	0.543	0.453, 0.631
	DDC (10^{-3} mm ² /s)	1.785	85.8	82.4	0.905	0.841, 0.949
	α	0.854	94.7	29.4	0.539	0.449, 0.627
Hypovascular vs. hypervascular	ADC (10^{-3} mm ² /s)	1.344	59.4	55.7	0.549	0.459, 0.636
	D_t (10^{-3} mm ² /s)	1.334	81.2	32.8	0.536	0.446, 0.624
	f (%)	18.934	69.6	72.1	0.762	0.679, 0.832
	D_p (10^{-3} mm ² /s)	37.484	76.8	44.3	0.608	0.518, 0.692
	DDC (10^{-3} mm ² /s)	2.293	13.0	95.1	0.513	0.424, 0.602
	α	0.710	82.6	47.5	0.664	0.576, 0.744
HCC vs. metastasis	ADC (10^{-3} mm ² /s)	1.427	70.5	39.1	0.507	0.409, 0.605
	D_t (10^{-3} mm ² /s)	1.334	90.2	23.9	0.530	0.431, 0.627
	f (%)	15.422	83.6	52.2	0.714	0.618, 0.797
	D_p (10^{-3} mm ² /s)	37.484	70.5	39.1	0.503	0.405, 0.602
	DDC (10^{-3} mm ² /s)	1.819	93.4	17.4	0.502	0.404, 0.600
	α	0.679	72.1	45.7	0.563	0.463, 0.658

ADC, apparent diffusion coefficient; D_t , true diffusion coefficient; D_p , pseudo-diffusion coefficient; f , perfusion fraction; DDC, distributed diffusion coefficient; α , intravoxel diffusion heterogeneity index; AUC, area under the receiver operating characteristic curve; CI, confidence interval

*Cysts were excluded, and hemangiomas were included in benign solid liver lesions

For the treated hepatic metastases that were surgically resected, we investigated the correlation between tumor necrosis and the DWI parameters, and α showed the most significant positive correlation with the degree of tumor necrosis after chemotherapy, followed by D_t . We assumed that viable cell density and tumor vascularity are reduced with tumor

necrosis progression, thereby increasing structural homogeneity resulting in an increasing α . Several prior studies have reported the potential value of α in the assessment of treatment response after chemotherapy [30–32]. In a study of 79 patients with rectal cancer, α was more useful than ADC and IVIM-derived parameters for predicting pathologic complete

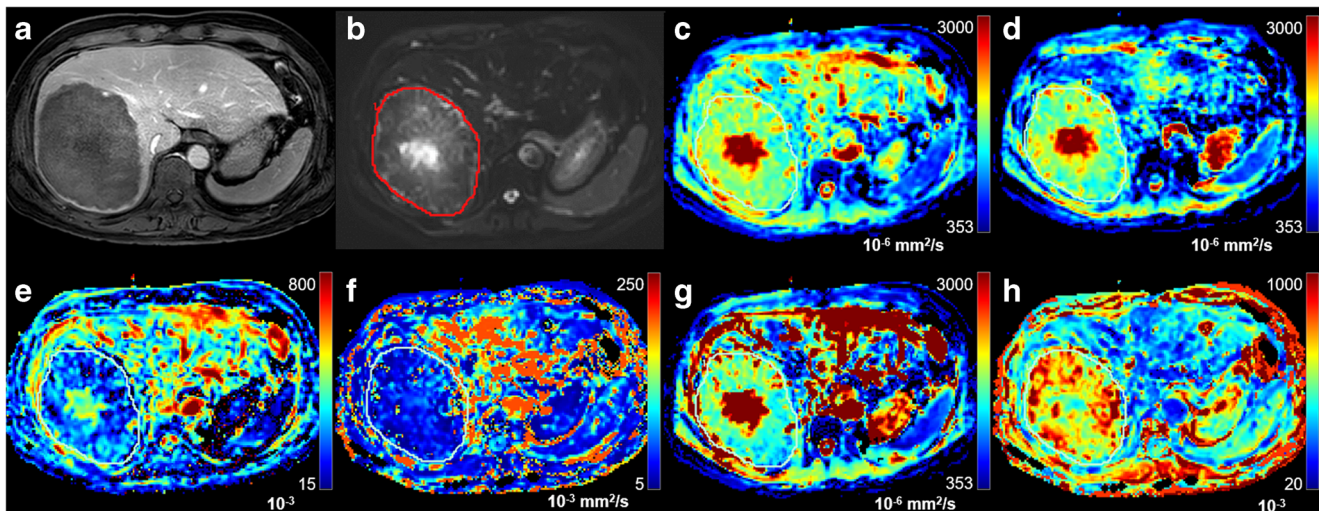


Fig. 5 Imaging of a 48-year-old man with treated colorectal liver metastasis. The pathologically proven degree of tumor necrosis was 85% after chemotherapy. (a) Axial T1-weighted image acquired during the portal phase showing a large hypovascular mass on the right hemiliver. (b) The region of interest was manually drawn on the hepatic

tumor on the diffusion-weighted image acquired with a b value of 0 s/mm² and copied onto (c–h) color maps. The values of (c) the ADC, (d) D_t , (e) f , (f) D_p , (g) DDC, and (h) α of metastasis were 1.82×10^{-3} mm²/s, 1.50×10^{-3} mm²/s, 24.72%, 33.16×10^{-3} mm²/s, 2.24×10^{-3} mm²/s, and 0.70, respectively

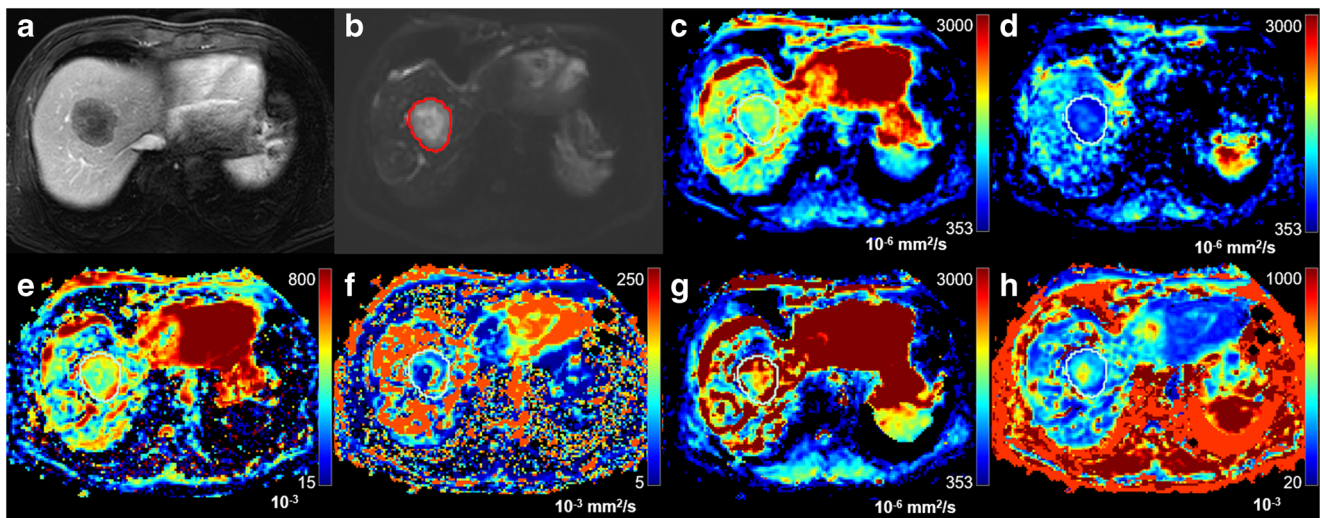


Fig. 6 Imaging of a 56-year-old man with treated liver metastasis from gastric cancer. The pathologically proven degree of tumor necrosis was 10% after chemotherapy. **a** Axial T1-weighted image acquired during the portal phase showing a hypovascular mass in liver segment VIII. **b** The region of interest was manually drawn on the hepatic tumor on the

diffusion-weighted image acquired with a b value of 0 s/mm^2 and copied onto (**c–h**) color maps. The values of (**c**) the ADC, (**d**) D_t , (**e**) f , (**f**) D_p , (**g**) DDC, and (**h**) α of metastasis were $1.64 \times 10^{-3} \text{ mm}^2/\text{s}$, $0.75 \times 10^{-3} \text{ mm}^2/\text{s}$, 44.10%, $80.73 \times 10^{-3} \text{ mm}^2/\text{s}$, $2.04 \times 10^{-3} \text{ mm}^2/\text{s}$, and 0.31, respectively

response [31]. In another study of 29 patients with metastatic abdominal and pelvic tumors, the α value significantly increased after treatment with vascular endothelial growth factor inhibitors [32]. Regarding the relationship between D_t and tumor necrosis, Chiaradia et al showed that tumor necrosis of colorectal cancer liver metastasis following systemic chemotherapy was correlated with a specific increase in D_t [22], which corroborates our results. However, because of the small number of patients and lack of serial inpatient comparison (before and after chemotherapy) in our study, larger prospective studies are warranted to generalize our results.

Several limitations of our study should be considered. First, an inherent selection bias may have affected the results because of the retrospective study design. Second, our patient cohort had a relatively small number of benign lesions, and most of solid benign FLLs were hemangiomas. Although the more critical issue is whether DWI can differentiate solid benign FLLs such as FNH or adenoma from malignancy, this could not be evaluated in this patient cohort. Third, because we included FLLs ≥ 2 cm to reduce measurement error, our results may not be applicable to smaller lesions. Fourth, we cannot guarantee the correspondence between the tumor slices assessed by the pathologist and the image slices where the DWI parameters were measured. Nevertheless, it might be meaningful that α measured at the largest tumor area reflects total tumor necrosis on pathologic examination. Fifth, as mentioned, the results regarding tumor necrosis and DWI parameters should be interpreted with caution because of the small number of patients and lack of serial comparison. Finally, the reproducibility of DWI parameters was not assessed. One major issue of diffusion MRI in the liver is

measurement error, caused by physiologic motion or differences in hardware. In addition, ROI measurements of the FLLs were performed by a single radiologist, which limits the reliability assessment of the DWI parameters.

In conclusion, our results indicate that the stretched exponential DWI model might be valuable for characterizing FLLs. The DDC demonstrated excellent diagnostic performance for differentiating malignant from benign lesions. We also suggest that α can be a promising indicator for evaluating the degree of necrosis in hepatic metastases after chemotherapy.

Funding The authors state that this work has not received any funding.

Compliance with ethical standards

Guarantor The scientific guarantor of this publication is Nieuw Seo.

Conflict of interest The authors of this manuscript declare no relationships with any companies whose products or services may be related to the subject matter of the article.

Statistics and biometry Nieuw Seo performed statistical analysis, who is one of the coauthors.

Informed consent Written informed consent was waived by the Institutional Review Board.

Ethical approval Institutional Review Board approval was obtained.

Methodology

- retrospective
- diagnostic or prognostic study
- performed at one institution

Publisher's note Springer Nature remains neutral with regard to jurisdictional claims in published maps and institutional affiliations.

References

- Parikh T, Drew SJ, Lee VS et al (2008) Focal liver lesion detection and characterization with diffusion-weighted MR imaging: comparison with standard breath-hold T2-weighted imaging. *Radiology* 246:812–822
- Taouli B, Koh DM (2010) Diffusion-weighted MR imaging of the liver. *Radiology* 254:47–66
- Taouli B, Vilgrain V, Dumont E, Daire JL, Fan B, Menu Y (2003) Evaluation of liver diffusion isotropy and characterization of focal hepatic lesions with two single-shot echo-planar MR imaging sequences: prospective study in 66 patients. *Radiology* 226:71–78
- Bruegel M, Holzapfel K, Gaa J et al (2008) Characterization of focal liver lesions by ADC measurements using a respiratory triggered diffusion-weighted single-shot echo-planar MR imaging technique. *Eur Radiol* 18:477–485
- Gourtsoyianni S, Papanikolaou N, Yarmenitis S, Maris T, Karantanas A, Gourtsoyiannis N (2008) Respiratory gated diffusion-weighted imaging of the liver: value of apparent diffusion coefficient measurements in the differentiation between most commonly encountered benign and malignant focal liver lesions. *Eur Radiol* 18:486–492
- Choi IY, Lee SS, Sung YS et al (2017) Intravoxel incoherent motion diffusion-weighted imaging for characterizing focal hepatic lesions: correlation with lesion enhancement. *J Magn Reson Imaging* 45:1589–1598
- Le Bihan D, Breton E, Lallemand D, Aubin ML, Vignaud J, Laval-Jeantet M (1988) Separation of diffusion and perfusion in intravoxel incoherent motion MR imaging. *Radiology* 168:497–505
- Yoon JH, Lee JM, Yu MH, Kiefer B, Han JK, Choi BI (2014) Evaluation of hepatic focal lesions using diffusion-weighted MR imaging: comparison of apparent diffusion coefficient and intravoxel incoherent motion-derived parameters. *J Magn Reson Imaging* 39:276–285
- Mulkern RV, Gudbjartsson H, Westin CF et al (1999) Multi-component apparent diffusion coefficients in human brain. *NMR Biomed* 12:51–62
- Clark CA, Le Bihan D (2000) Water diffusion compartmentation and anisotropy at high b values in the human brain. *Magn Reson Med* 44:852–859
- Bennett KM, Schmainda KM, Bennett RT, Rowe DB, Lu H, Hyde JS (2003) Characterization of continuously distributed cortical water diffusion rates with a stretched-exponential model. *Magn Reson Med* 50:727–734
- Seo N, Chung YE, Park YN, Kim E, Hwang J, Kim MJ (2018) Liver fibrosis: stretched exponential model outperforms mono-exponential and bi-exponential models of diffusion-weighted MRI. *Eur Radiol* 28:2812–2822
- Bai Y, Lin Y, Tian J et al (2016) Grading of gliomas by using monoexponential, biexponential, and stretched exponential diffusion-weighted MR imaging and diffusion kurtosis MR imaging. *Radiology* 278:496–504
- Winfield JM, Orton MR, Collins DJ et al (2017) Separation of type and grade in cervical tumours using non-mono-exponential models of diffusion-weighted MRI. *Eur Radiol* 27:627–636
- Lin M, Yu X, Chen Y et al (2017) Contribution of mono-exponential, bi-exponential and stretched exponential model-based diffusion-weighted MR imaging in the diagnosis and differentiation of uterine cervical carcinoma. *Eur Radiol* 27:2400–2410
- Liu X, Zhou L, Peng W, Wang H, Zhang Y (2015) Comparison of stretched-exponential and monoexponential model diffusion-weighted imaging in prostate cancer and normal tissues. *J Magn Reson Imaging* 42:1078–1085
- Hectors SJ, Semaan S, Song C et al (2018) Advanced diffusion-weighted imaging modeling for prostate cancer characterization: correlation with quantitative histopathologic tumor tissue composition—a hypothesis-generating study. *Radiology* 286:918–928
- Anderson SW, Barry B, Soto J, Ozonoff A, O'Brien M, Jara H (2014) Characterizing non-Gaussian, high b-value diffusion in liver fibrosis: stretched exponential and diffusional kurtosis modeling. *J Magn Reson Imaging* 39:827–834
- Hu Y, Tang H, Li H et al (2018) Assessment of different mathematical models for diffusion-weighted imaging as quantitative biomarkers for differentiating benign from malignant solid hepatic lesions. *Cancer Med*. <https://doi.org/10.1002/cam4.1535>
- Cui Y, Zhang XP, Sun YS, Tang L, Shen L (2008) Apparent diffusion coefficient: potential imaging biomarker for prediction and early detection of response to chemotherapy in hepatic metastases. *Radiology* 248:894–900
- Koh DM, Scurr E, Collins D et al (2007) Predicting response of colorectal hepatic metastasis: value of pretreatment apparent diffusion coefficients. *AJR Am J Roentgenol* 188:1001–1008
- Chiaradia M, Baranes L, Van Nhieu JT et al (2014) Intravoxel incoherent motion (IVIM) MR imaging of colorectal liver metastases: are we only looking at tumor necrosis? *J Magn Reson Imaging* 39:317–325
- Bruix J, Sherman M (2011) Management of hepatocellular carcinoma: an update. *Hepatology* 53:1020–1022
- Danet IM, Semelka RC, Leonardou P et al (2003) Spectrum of MRI appearances of untreated metastases of the liver. *AJR Am J Roentgenol* 181:809–817
- Seale MK, Catalano OA, Saini S, Hahn PF, Sahani DV (2009) Hepatobiliary-specific MR contrast agents: role in imaging the liver and biliary tree. *Radiographics* 29:1725–1748
- Qian LJ, Zhu J, Zhuang ZG, Xia Q, Liu Q, Xu JR (2013) Spectrum of multilocular cystic hepatic lesions: CT and MR imaging findings with pathologic correlation. *Radiographics* 33:1419–1433
- Chandarana H, Lee VS, Hecht E, Taouli B, Sigmund EE (2011) Comparison of biexponential and monoexponential model of diffusion weighted imaging in evaluation of renal lesions: preliminary experience. *Invest Radiol* 46:285–291
- Woo S, Lee JM, Yoon JH, Joo I, Han JK, Choi BI (2014) Intravoxel incoherent motion diffusion-weighted MR imaging of hepatocellular carcinoma: correlation with enhancement degree and histologic grade. *Radiology* 270:758–767
- Lee Y, Lee SS, Kim N et al (2015) Intravoxel incoherent motion diffusion-weighted MR imaging of the liver: effect of triggering methods on regional variability and measurement repeatability of quantitative parameters. *Radiology* 274:405–415
- Bedair R, Priest AN, Patterson AJ et al (2017) Assessment of early treatment response to neoadjuvant chemotherapy in breast cancer using non-mono-exponential diffusion models: a feasibility study comparing the baseline and mid-treatment MRI examinations. *Eur Radiol* 27:2726–2736
- Zhu HB, Zhang XY, Zhou XH et al (2017) Assessment of pathological complete response to preoperative chemoradiotherapy by means of multiple mathematical models of diffusion-weighted MRI in locally advanced rectal cancer: a prospective single-center study. *J Magn Reson Imaging* 46:175–183
- Orton MR, Messiou C, Collins D et al (2016) Diffusion-weighted MR imaging of metastatic abdominal and pelvic tumours is sensitive to early changes induced by a VEGF inhibitor using alternative diffusion attenuation models. *Eur Radiol* 26:1412–1419